Mechanisms for Pressure-Induced Isostructural Phase Transitions in EuO

Jacques K. Desmarais,[1,2,3,4,*] Alessandro Erba,[1] Yuanming Pan,[3] Bartolomeo Civalleri,[1] and John S. Tse[4,†]
[1]Dipartimento di Chimica e NIS centro interdipartimentale, Università di Torino, Via P. Giuria 7, 10125 Torino, Italy
[2]Equipe de Chimie Physique, IPREM UMR5254, Université de Pau et des Pays de lAdour, 64053, Pau, CEDEX 9, France
[3]Department of Geological Sciences, University of Saskatchewan, Saskatoon, Saskatchewan S7N 5E2, Canada
[4]Department of Physics and Engineering Physics, University of Saskatchewan, Saskatoon, Saskatchewan S7N 5E2, Canada

(Received 5 January 2021; revised 1 March 2021; accepted 22 April 2021; published 12 May 2021)

We study pressure-induced isostructural electronic phase transitions in the prototypical mixed valence and strongly correlated material EuO using the global-hybrid density functional theory. The simultaneous presence in the valence of highly localized d- and f-type bands and itinerant s- and p-type states, as well as the half-filled f-type orbital shell with seven unpaired electrons on each Eu atom, have made the description of the electronic features of this system a challenge. The electronic band structure, density of states, and atomic oxidation states of EuO are analyzed in the 0–50 GPa pressure range. An insulator-to-metal transition at about 12 GPa of pressure was identified. The second isostructural transition at approximately 30–35 GPa, previously believed to be driven by an oxidation from Eu(II) to Eu(III), is shown instead to be associated with a change in the occupation of the Eu d orbitals, as can be determined from the analysis of the corresponding atomic orbital populations. The Eu d band is confined by the surrounding oxygens and split by the crystal field, which results in orbitals of e_g symmetry (i.e., $d_{x^2-y^2}$ and $d_{2z^2-x^2-y^2}$, pointing along the Eu-O direction) being abruptly depopulated at the transition as a means to alleviate electron-electron repulsion in the highly compressed structures.

DOI: 10.1103/PhysRevLett.126.196404

Strongly correlated materials are characterized by partially occupied d- and/or f-type bands with highly localized unpaired electrons [1,2]. The hybridization of these bands with more itinerant s-, p-, and d-type ones causes competing valence states, whose superposition results in so-called mixed valency [3–6]. In these materials, the valence state's occupation can be effectively modulated by external factors, such as temperature and pressure [7–14]. The description of the highly localized d- and/or f-type bands, in combination with the more itinerant s, p, and d orbitals is particularly challenging from the point of view of conventional Kohn-Sham density functional theory (KS-DFT). One common feature of mixed-valence materials is the occurrence of isostructural volume collapses (IVCs) [15]. An enigmatic and unresolved problem in high pressure physics is the suggestion of pressure-induced changes on the valence states. EuO is a prototypical example of this phenomenon. It has been suggested that upon compression, the Eu atoms transit from a +2 to a +3 oxidation state and then reenter into the +2 state [3,16–18]. Three phase transitions occur in EuO within the pressure range from 0 to 60 GPa. They include two IVC (insulator-to-metal and metal-to-metal) transitions at around 10–15 and 30–35 GPa, respectively, and an NaCl (B1) to CsCl (B2) structural transition at around 50–60 GPa [12,19–21]. So far, no theoretical calculation has been able to reproduce the mechanism of the metal-to-metal IVC transition, despite this was the first one to be observed more than 50 years ago [22].

Sophisticated theoretical frameworks are required for a proper description of strongly correlated lanthanide oxides. These methods include the empirical Hubbard on-site DFT + U method [23–25], the SIC (self-interaction corrected) local spin-density approximation (SIC-LSDA) [15,17,26], and many-body perturbation theory in the G_0W_0@LSDA + U and GW_0@LSDA + U approximations [27,28]. However, these methods introduce additional parameters to the theory (for example, values of the on-site Hubbard terms U for each orbital at the different crystallographic sites). An alternative method is to employ hybrid density functionals, such the global-hybrid functionals [1,29] or range-separated hybrid functionals [30]. These methods require the explicit specification of the fraction of exact nonlocal Fock exchange and, possibly, also the value for the range separation parameter. The approach introducing the least empiricism is the one-parameter global-hybrid functional one, which is used here (PBE0) [31]. The main issues to resolve are the electronic origins of the volume collapse associated with the IVC at 30–35 GPa and the "apparent" change of the Eu valence state from +2 to +3. As the results show below, we were able to reproduce the insulator-to-metal transition at 10–15 GPa and explain the elusive IVC at 30–35 GPa within the straightforward band structure picture.

Calculations are mainly performed with a developmental version of the CRYSTAL17 code [32,33], which is based on a periodic linear combination of atomic orbitals (LCAO)

framework, whereby Bloch functions are expanded in a set of Gaussian-type functions up to angular momentum $l = 4$ (i.e., g-type atomic orbitals) [34]. Details on the computational setup can be found in the Supplemental Material [35] (see also Refs. [36–57] therein). Additional calculations were performed with standard plane-wave codes using gradient-corrected, as well as hybrid functionals, and are provided in Ref. [35]. The main body predominantly discusses results obtained from the CRYSTAL17 LCAO calculations.

The crystal structure of the B1 phase of EuO was fully optimized in the absence of external pressure (with obtained volume denoted as V_0 and energy E_0). The Eu atoms are in an octahedral environment, surrounded by O atoms at the vertices of the octahedron (see top right panel of Fig. 1). It is worth noting that the octahedral crystal field splits the d band of Eu into e_g states pointing along the Eu-O bonds, and t_{2g} states pointing between O atoms (i.e., along the Eu-Eu direction).

Total energy calculations were subsequently performed at compressed volumes, corresponding to the range from $V/V_0 = 1.00$ to 0.75. Energies are reported in the top left panel of Fig. 1. The energy-volume relation appears rather continuous to the naked eye. The plane-wave calculations produced a similar smooth trend (see Fig. S2 of the Supplemental Material [35]). While two discontinuities are numerically predicted in the energy-volume relation at the points denoted by the vertical dashed lines, their magnitude is small, and it is not obvious to unambiguously assign volumes for the transitions solely from the analysis of the total energy. It is insightful to also look for discontinuities in the electronic state, from analysis of the band structure and orbital populations. In particular, as discussed further below, present LCAO calculations allow for the unambiguous decomposition of the band structure of EuO in terms of contributions from individual atomic orbitals, and thus for the identification and explanation of the mechanisms of the isostructural phase transitions.

The left middle panel in Fig. 1 demonstrates the vanishing indirect band gap at the volume $V/V_0 = 0.881$, associated with the insulator-to-metal transition. The calculation confirms the earlier proposal for the metallization from the study of the UV absorption spectra [22]. Further compressing the system, discontinuities are observed in atomic orbital populations: the bottom left panel of Fig. 1 reports populations of d-type bands of Eu atoms in EuO, showing an initial increase in population, followed by a discontinuity at the volume $V/V_0 = 0.798$, and finally an abrupt depopulation for the most compressed structures. Populations of bands of s, p, or f character instead do not show such change in

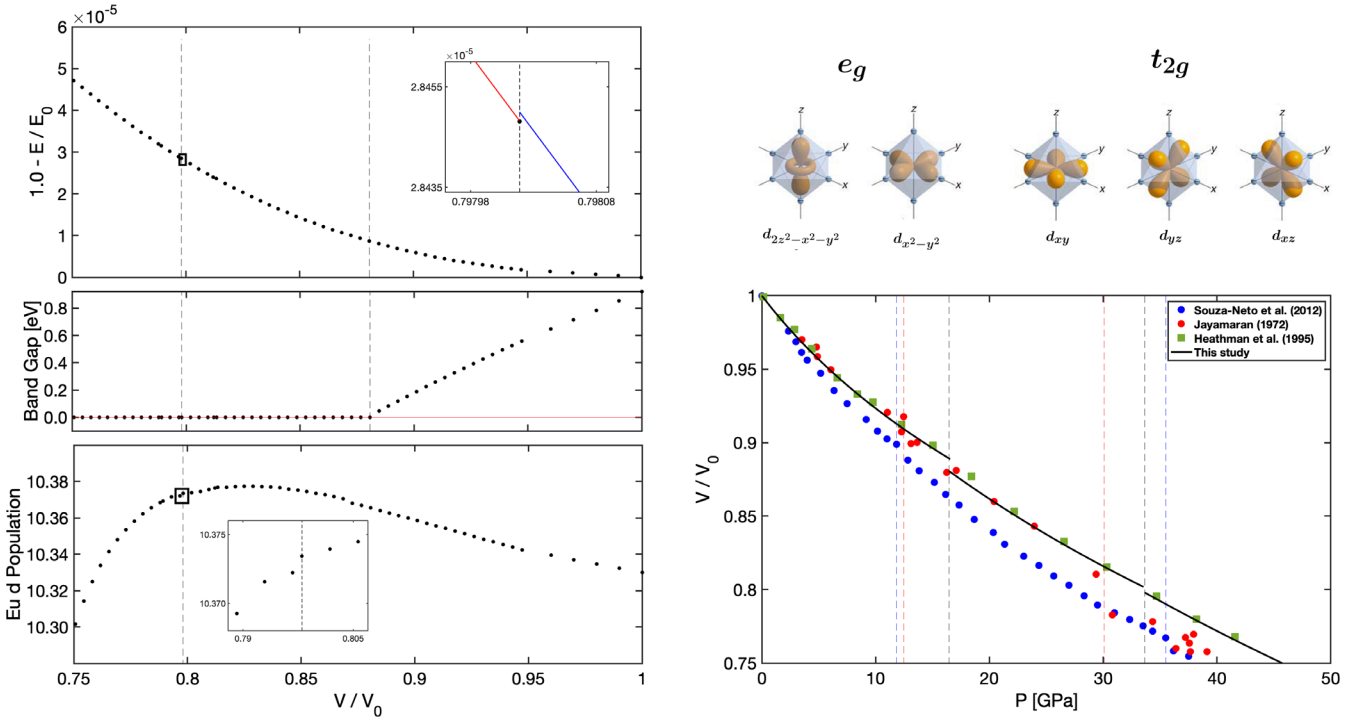

FIG. 1. (Left top panel) Calculated energy-volume relation. (Left middle panel) band gap of EuO as a function of volume. (Left bottom panel) Population of d-type bands of Eu atoms in EuO as a function of volume. (Right top panel) d orbitals of e_g symmetry point along the Eu-O bonds of the EuO octahedron and d orbitals of t_{2g} symmetry point between O atoms (along the Eu-Eu direction). (Right bottom panel) Pressure-volume equation of state of EuO as fitted to the calculations in the present study (black line) and measured in previous experiments (colored symbols) [3,22,58]. Transition volumes and pressures are marked with dashed vertical lines, with colors matching the symbols.

behavior with compression, and are found to vary consistently, apart from a small discontinuity, again at the volume $V/V_0 = 0.798$ (see Fig. S10 [35]). The discontinuity can also be observed from the magnetic moment of Eu (see Fig. S9 [35]). The analysis of the atomic orbital populations thus allows us to define a second phase transition at the volume $V/V_0 = 0.798$. Calculations performed with different flavors of hybrid DFT (such as the HSE06 [59] and B3LYP [60] exchange-correlation functionals) also reproduce this transition (see Fig. S8 [35]).

Based on the insight discussed above into the discontinuity of relevant electronic features, we are now able to correspondingly branch the energy-volume relation into three segments, and fit each of them to third-order Birch-Murnaghan equations of state (EOS) to obtain the corresponding pressure-volume relation, reported in the right bottom panel of Fig. 1. The fitting indeed yields two volume collapses at the pressures of 16 GPa (for the insulator-to-metal transition) and 33 GPa (for the metal-to-metal transition), which compares well to the corresponding values from previous experiments in the colored symbols.

We now analyze more closely the electronic features of EuO at the 33 GPa IVC transition. It was mentioned above that, with increasing pressure, all orbital populations of Eu vary consistently, apart from a small discontinuity at the 33 GPa IVC (Fig. S10 [35]) with the exception of the d-type bands, which instead show an abrupt decrease in population at pressures beyond the transition. The calculated projected densities of states (PDOSS) reported in Fig. S12 [35] show a similar behavior but in more detail. It is seen that while the Eu s, p, and f PDOSS vary linearly with increasing pressure, a marked change in behavior is instead observed in the Eu d PDOSS close to the transition pressure. Significantly, the initial increase of the height and sharpening of the bandwidth of the peak of the Eu d PDOSS below 33 GPa (blue tones in Fig. S12 [35]), transform into the decrease of the height and broadening of the bandwidth of the Eu d PDOSS above 33 GPa (red tones in the figure).

As anticipated, an explanation for the discontinuity in the behavior of the d band upon compression can be found by taking into account the splitting into e_g and t_{2g} subsets, with the help of Fig. 2. At pressures below the second IVC—that is to say, the metal-to-metal transition at 33 GPa—[blue tones in Figs. 2(a) and 2(b)], all of the d states at the Fermi level are of t_{2g} symmetry. At pressures at and above the metal-to-metal IVC [red tones in Figs. 2(a) and 2(b)], a finite DOSS from the e_g states emerges at the Fermi level. At the same time, such e_g states get abruptly depopulated at the transition [see Figs. 2(c) and 2(d)] compared to t_{2g} states. Given that the e_g states point directly along the Eu-O bonds of the EuO octahedron, their depopulation helps to alleviate electron-electron repulsion in the highly compressed structures. On the other hand, the states of t_{2g}

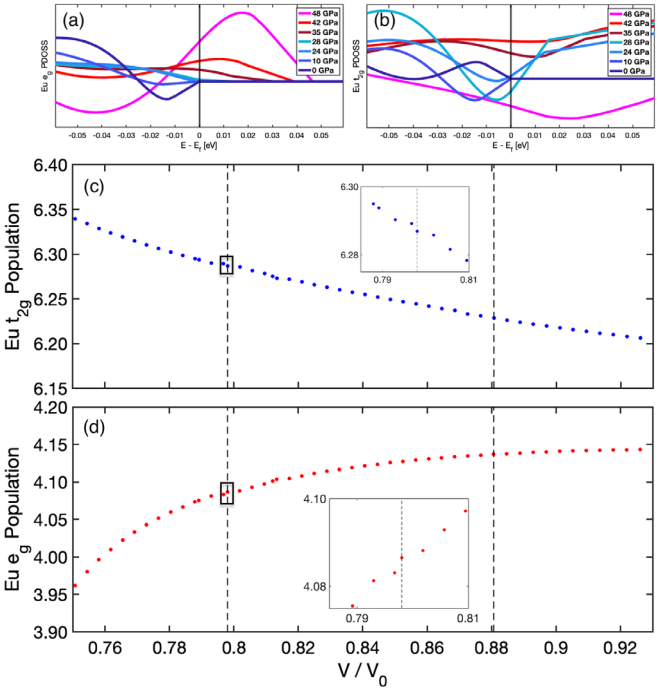

FIG. 2. (a) and (b) Evolution with pressure (blue tones and red tones below and above the metal-to-metal transition, respectively) of PDOSS of d orbitals of Eu of (a) e_g and (b) t_{2g} symmetry. (c) and (d) Orbital population of d-type orbitals of Eu as a function of pressure. The Eu atom is in an octahedral environment with the e_g (and t_{2g}) sets pointing towards (between) O atoms.

symmetry point along the Eu-Eu direction for two Eu atoms lying far away in adjoining cells. The t_{2g} states are hence stabilized by pressure compared to the e_g ones, and are seen to consistently increase in population across the metal-to-metal transition [see Fig. 2(c)]. To wrap it up, the emergence of states of e_g symmetry at the Fermi level allows for their abrupt depopulation at the metal-to-metal transition, correspondingly leading to a volume collapse.

Electronic insight from the experiments on these transitions is scarce, a notable exception being the experimental study by Souza-Neto *et al.* [3]. In the range 0–30 GPa, an increase in the cationic charge of Eu as a function of pressure was inferred from Eu $2p$ (L edge) x-ray absorption near-edge structure (XANES) spectroscopy and from Mössbauer isomer shifts (IS) derived from nuclear forward scattering [3]. A charge depletion for Eu of 0.25 e was deduced from the IS and 0.13 e from the XANES. Table S1 of the Supplemental Material [35] summarizes the computed changes in orbital populations and atomic charges in the same 0–30 GPa pressure range. Atomic populations and charges are computed with the Mulliken scheme as well as with the more accurate iterative Hirschfeld-I approach [61–63]. Let us stress that, while absolute values of computed atomic charges are known to critically depend on the particular partitioning scheme adopted, trends such as those discussed below are typically less sensitive.

Table S1 [35] shows that the change in the electronic structure in EuO is dominated by charge depletion from s- and p-type bands in Eu and the concomitant charge accumulation in p-type bands of O. As anticipated, charge differences computed with the Mulliken and Hirschfeld-I approaches are similar, with deviations smaller than 6%. Crucially, no significant charge transfer from the Eu $4f$ to $5d$ orbitals is predicted. Indeed, in the first report on the high-pressure behavior of EuO, the isostructural transitions at 12 and 33 GPa were attributed to a $4f \rightarrow 5d$ electron transfer. The hypothesis of a transfer of electrons from the localized $4f$ to delocalized $5d$ orbitals may have led to the interpretation of an "apparent" increase of the Eu oxidation state from +2 to +3 [22]. Although the calculated trends for the total charge are consistent with the change in oxidation state inferred from the experiments, they also show only very minor changes in the population of the d orbitals (by +0.05 e, see bottom left panel of Fig. 1) and of f orbitals (by −0.05 e, see Fig. S10 of the Supplemental Material [35]). Therefore, such a minor charge transfer cannot account for the 7 eV shift in the XANES absorption band to higher energy [3] as the principal evidence of increased oxidation state.

The observed shift in the absorption peak in the Eu L-XANES of compressed EuO can now be analyzed [3]. The core-hole excitation intensities of x-ray absorption are dominated by the local site of the absorbing center and satisfy the dipole selection rules. In this case, the lowest energy XANES peak is mainly due to the electronic transitions of the Eu $2p$ core electrons into the empty bands, predominantly of d type, confined by the crystal field from the nearest neighbor oxygen atoms and split into e_g and t_{2g} levels. This phenomenon is known as "shape resonance" and has been well studied in many systems, including oxides [64,65]. In the experiment, the absorption band can be deconvoluted to two bands. At low pressure, the lower energy peak is more intense than the higher energy one and the spectral profile is typical of a Eu(II) species. As the pressure increases, the intensity of the second peak increases relative to the first. Incidentally, at 40 GPa, above the IVC, the XANES profile of the higher energy peak resembles that of an Eu(III) species, which led to the interpretation of an increased oxidation state. However, it is important to note that the excitation energy of x-ray absorption is proportional to the difference of the band energies of the excited and hole states. The experimental spectra show that the mean positions (i.e., excitation energy) of the bands do not change with compression. This is contrary to the expectation that the energy of the initial orbital (i.e., Eu $2p$ core state) would be affected from a significant increase of the oxidation state.

A comparison of the calculated DOS of the empty t_{2g} and e_g orbitals is shown in Fig. 3 (and also Fig. S13 [35], which includes more pressure points). The e_g band lies slightly higher in energy with respect to the much broader t_{2g} band.

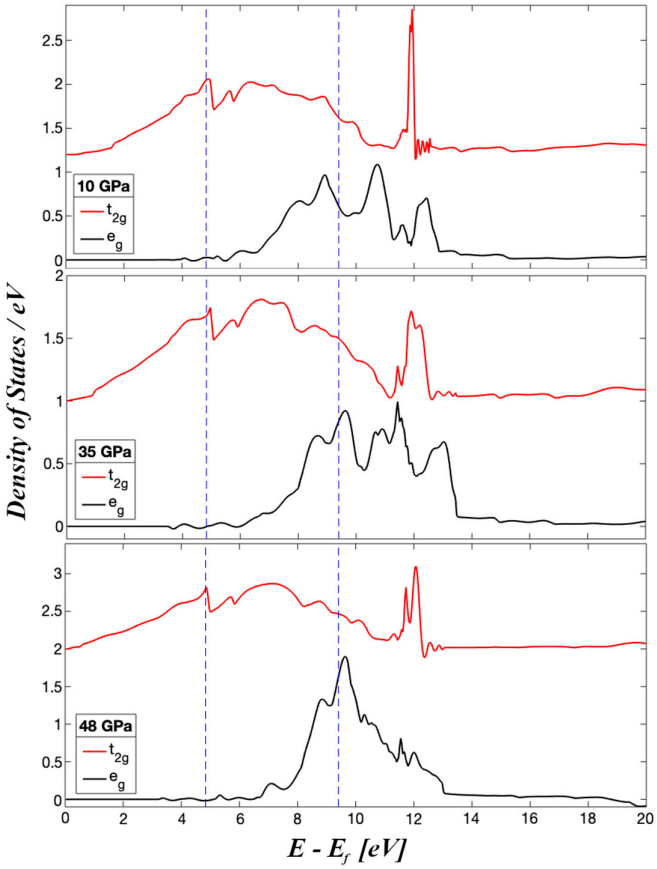

FIG. 3. Calculated total DOS (sum of spin-up and spin-down contributions) of the t_{2g} and e_g band at selected pressures. Vertical blue dashed lines (separated by 5 eV) are a guide to the eye.

In addition, a sharp and narrow band is predicted for the t_{2g} species at high energy. The energy difference between the maxima of the t_{2g} and e_g bands is about 5 eV (see blue dashed lines in the figures) and does not change much with pressure. This value may be compared with the observed separation of 7 eV between the low and high energy bands in the experimental spectra. Therefore, it is not unreasonable to associate the lower energy band as being due to excitations of Eu $2p$ electrons to the t_{2g} level and the higher band to the e_g level. As the pressure is increased, there is no substantial change in the DOS profiles until 48 GPa, at which point it can be seen in Fig. 3 and Fig. S13 [35] that the e_g band becomes compressed with a much narrower width. If oscillator strength is related to the DOS, and therefore to the intensity of the high energy peak, which is still around 5 eV from the lower energy peak, then the corresponding peak in the spectral profile is also expected to be strongly enhanced, as observed in the experiment. From the analysis of the calculated charge transfer and the DOS profiles, we can conclude that there is no noticeable change in the Eu oxidation state. The reported variation on the spectral features in the XANES is due to a substantial change in the DOS of the empty e_g band. The volume

collapse associated with the isostructural transition at 33 GPa can be explained using a similar picture. Above the insulator-to-metal transition at 12 GPa, apart from a slight transfer of electrons from Eu to O, there is no fundamental change in the electronic structure. However, the population of the t_{2g} orbitals gradually increases. Noting that the t_{2g} set is comprised of d_{xz}, d_{yz}, and d_{xy} orbitals pointing between the O atoms, accumulation of charge density away from direct pointing positions helps to alleviate electron-electron repulsion and favors an isostructural volume reduction at 33 GPa, in response to the abrupt depopulation of e_g states.

In summary, we show that the two IVCs in the B1 phase of EuO can be explained within the standard KS-DFT approach with a self-interaction correction included in the global-hybrid functional. The pressure dependent electronic structure is related to changes in the electron density distribution. In particular, the elusive metal-to-metal transition is rationalized in terms of the different behaviour of the crystal field split t_{2g} and e_g d-type bands. We show the usefulness of reliable indicators based on the population of individual atomic orbitals within LCAO calculations in the analysis of the band structure as a means to interpret phase transitions at high pressure. Detailed orbital mechanisms are illustrated, which explain the occurrence of the IVCs in EuO that are also common to other mixed valence materials. The work suggests proceeding with caution when interpreting high-pressure experimental spectra in terms of ambient pressure standards. An exact analog to the high-pressure electronic state may not exist at ambient conditions, in which case interpretation of the experiment can only be guided with the help of first-principles calculations.

The authors thank Laboratory Computing Resource Center—Argonne National Laboratory and Compute Canada for the allocation of computer resources, and Dr. N. Zarifi for the LAPW results. J. K. D. is grateful to the National Science and Engineering Research Council (NSERC) of the government of Canada for a postdoctoral fellowship (Grant No. 545643) and a Vanier Scholarship (Grant No. 360289).

*jacqueskontak.desmarais@unito.it
†john.tse@usask.ca

[1] K. E. El-Kelany, C. Ravoux, J. K. Desmarais, P. Cortona, Y. Pan, J. S. Tse, and A. Erba, Phys. Rev. B **97**, 245118 (2018).
[2] P. Rivero, I. P. R. Moreira, G. E. Scuseria, and F. Illas, Phys. Rev. B **79**, 245129 (2009).
[3] N. M. Souza-Neto, J. Zhao, E. E. Alp, G. Shen, S. V. Sinogeikin, G. Lapertot, and D. Haskel, Phys. Rev. Lett. **109**, 026403 (2012).
[4] C. Varma, Rev. Mod. Phys. **48**, 219 (1976).
[5] Y. Matsumoto, S. Nakatsuji, K. Kuga, Y. Karaki, N. Horie, Y. Shimura, T. Sakakibara, A. H. Nevidomskyy, and P. Coleman, Science **331**, 316 (2011).
[6] M. Okawa, M. Matsunami, K. Ishizaka, R. Eguchi, M. Taguchi, A. Chainani, Y. Takata, M. Yabashi, K. Tamasaku, Y. Nishino *et al.*, Phys. Rev. Lett. **104**, 247201 (2010).
[7] J. Arvanitidis, K. Papagelis, S. Margadonna, K. Prassides, and A. N. Fitch, Nature (London) **425**, 599 (2003).
[8] M. M. Abd-Elmeguid, C. Sauer, and W. Zinn, Phys. Rev. Lett. **55**, 2467 (1985).
[9] M. Dzero, M. R. Norman, I. Paul, C. Pépin, and J. Schmalian, Phys. Rev. Lett. **97**, 185701 (2006).
[10] I. Jarrige, H. Yamaoka, J.-P. Rueff, J.-F. Lin, M. Taguchi, N. Hiraoka, H. Ishii, K.-D. Tsuei, K. Imura, T. Matsumura *et al.*, Phys. Rev. B **87**, 115107 (2013).
[11] J. R. L. Mardegan, G. Fabbris, L. S. I. Veiga, C. Adriano, M. A. Avila, D. Haskel, and C. Giles, Phys. Rev. B **88**, 144105 (2013).
[12] H. Yamaoka, N. Tsujii, M.-T. Suzuki, Y. Yamamoto, I. Jarrige, H. Sato, J.-F. Lin, T. Mito, J. Mizuki, H. Sakurai *et al.*, Sci. Rep. **7**, 5846 (2017).
[13] N. Souza-Neto, D. Haskel, R. dos Reis, and F. Gandra, High Press. Res. **36**, 360 (2016).
[14] H. Yamaoka, N. Tsujii, Y. Yamamoto, Y. Michiue, J.-F. Lin, N. Hiraoka, H. Ishii, K.-D. Tsuei, and J. Mizuki, Phys. Rev. B **97**, 085106 (2018).
[15] L. Petit, Z. Szotek, M. Lüders, W. M. Temmerman, and A. Svane, Phys. Rev. B **90**, 035110 (2014).
[16] A. Melville, T. Mairoser, A. Schmehl, T. Birol, T. Heeg, B. Holländer, J. Schubert, C. Fennie, and D. Schlom, Appl. Phys. Lett. **102**, 062404 (2013).
[17] L. Petit, Z. Szotek, M. Lüders, and A. Svane, J. Phys. Condens. Matter **28**, 223001 (2016).
[18] J. O. Kafader, M. Ray, and C. C. Jarrold, J. Chem. Phys. **143**, 034305 (2015).
[19] A. Schmehl, V. Vaithyanathan, A. Herrnberger, S. Thiel, C. Richter, M. Liberati, T. Heeg, M. Röckerath, L. F. Kourkoutis, S. Mühlbauer *et al.*, Nat. Mater. **6**, 882 (2007).
[20] H. G. Zimmer, K. Takemura, K. Syassen, and K. Fischer, Phys. Rev. B **29**, 2350 (1984).
[21] N. Zarifi, Ph.D. thesis, University of Saskatchewan, 2015.
[22] A. Jayaraman, Phys. Rev. Lett. **29**, 1674 (1972).
[23] P. Giannozzi, S. Baroni, N. Bonini, M. Calandra, R.Car, C. Cavazzoni, D. Ceresoli, G. L. Chiarotti, M. Cococcioni, I. Dabo *et al.*, J. Phys. Condens. Matter **21**, 395502 (2009).
[24] C. Loschen, J. Carrasco, K. M. Neyman, and F. Illas, Phys. Rev. B **75**, 035115 (2007).
[25] D. Richard, E. L. Muñoz, M. Rentería, L. A. Errico, A. Svane, and N. E. Christensen, Phys. Rev. B **88**, 165206 (2013).
[26] L. Petit, A. Svane, Z. Szotek, and W. M. Temmerman, Phys. Rev. B **72**, 205118 (2005).
[27] H. Jiang, P. Rinke, and M. Scheffler, Phys. Rev. B **86**, 125115 (2012).
[28] H. Jiang, R. I. Gomez-Abal, P. Rinke, and M. Scheffler, Phys. Rev. Lett. **102**, 126403 (2009).
[29] J. Graciani, A. M. Marquez, J. J. Plata, Y. Ortega, N. C. Hernandez, A. Meyer, C. M. Zicovich-Wilson, and J. F. Sanz, J. Chem. Theory Comput. **7**, 56 (2011).

[30] P. J. Hay, R. L. Martin, J. Uddin, and G. E. Scuseria, J. Chem. Phys. **125**, 034712 (2006).
[31] C. Adamo and V. Barone, J. Chem. Phys. **110**, 6158 (1999).
[32] R. Dovesi, A. Erba, R. Orlando, C. M. Zicovich-Wilson, B. Civalleri, L. Maschio, M. Rérat, S. Casassa, J. Baima, S. Salustro *et al.*, WIREs Comput. Mol. Sci. **8**, e1360 (2018).
[33] A. Erba, J. Baima, I. Bush, R. Orlando, and R. Dovesi, J. Chem. Theory Comput. **13**, 5019 (2017).
[34] J. Desmarais, A. Erba, and R. Dovesi, Theor. Chem. Acc. **137**, 28 (2018).
[35] See Supplemental Material at http://link.aps.org/supplemental/10.1103/PhysRevLett.126.196404 for the computational details of the LCAO calculations, a discussion providing evidence for the excellent quality of the adopted basis set expansion, a discussion on the effect of including a variational treatment of inner valence states to the calculations, as well as additional plane-wave calculations, and further plots for the orbital populations as well as the density of states as a function of pressure.
[36] M. Dolg, H. Stoll, and H. Preuss, J. Chem. Phys. **90**, 1730 (1989).
[37] All optimized basis sets are available at http://www.crystal.unito.it/basis-sets.php.
[38] X. Cao and M. Dolg, J. Chem. Phys. **115**, 7348 (2001).
[39] TURBOMOLE V7.3 2018, a development of University of Karlsruhe and Forschungszentrum Karlsruhe GmbH, 1989-2007, TURBOMOLE GmbH, since 2007; available from http://www.turbomole.com.
[40] K. Doll, Comput. Phys. Commun. **137**, 74 (2001).
[41] K. Doll, V. Saunders, and N. Harrison, Int. J. Quantum Chem. **82**, 1 (2001).
[42] K. Doll, R. Dovesi, and R. Orlando, Theor. Chem. Acc. **112**, 394 (2004).
[43] K. Doll, R. Dovesi, and R. Orlando, Theor. Chem. Acc. **115**, 354 (2006).
[44] J. K. Desmarais, J.-P. Flament, and A. Erba, J. Phys. Chem. Lett. **10**, 3580 (2019).
[45] J. K. Desmarais, J.-P. Flament, and A. Erba, J. Chem. Phys. **151**, 074107 (2019).
[46] J. K. Desmarais, J.-P. Flament, and A. Erba, Phys. Rev. B **101**, 235142 (2020).
[47] J. K. Desmarais, J.-P. Flament, and A. Erba, Phys. Rev. B **102**, 235118 (2020).
[48] J. K. Desmarais, Ph. D. thesis, University of Saskatchewan and University of Turin, 2020.
[49] H. Wang, C. Schuster, and U. Schwingenschlögl, Chem. Phys. Lett. **524**, 68 (2012).
[50] J. P. Perdew, K. Burke, and M. Ernzerhof, Phys. Rev. Lett. **77**, 3865 (1996).
[51] G. Kresse and J. Hafner, Phys. Rev. B **47**, 558 (1993).
[52] G. Kresse and J. Furthmüller, Phys. Rev. B **54**, 11169 (1996).
[53] P. Blaha, K. Schwarz, P. Sorantin, and S. Trickey, Comput. Phys. Commun. **59**, 399 (1990).
[54] X. Wan, J. Dong, and S. Y. Savrasov, Phys. Rev. B **83**, 205201 (2011).
[55] R. Gillen, S. J. Clark, and J. Robertson, Phys. Rev. B **87**, 125116 (2013).
[56] R. Nelson, C. Ertural, J. George, V. L. Deringer, G. Hautier, and R. Dronskowski, J. Comput. Chem. **41**, 1931 (2020).
[57] S. Maintz, V. L. Deringer, A. L. Tchougréeff, and R. Dronskowski, J. Comput. Chem. **37**, 1030 (2016).
[58] S. Heathman, T. Le Bihan, S. Darracq, C. Abraham, D. De Ridder, U. Benedict, K. Mattenberger, and O. Vogt, J. Alloys Compd. **230**, 89 (1995).
[59] J. Heyd, G. E. Scuseria, and M. Ernzerhof, J. Chem. Phys. **124**, 219906 (2006).
[60] A. D. Becke, J. Chem. Phys. **98**, 5648 (1993).
[61] F. L. Hirshfeld, Theor. Chim. Acta **44**, 129 (1977).
[62] P. Bultinck, C. Van Alsenoy, P. W. Ayers, and R. Carbó-Dorca, J. Chem. Phys. **126**, 144111 (2007).
[63] C. Zicovich-Wilson, M. Hô, A. Navarrete-López, and S. Casassa, Theor. Chem. Acc. **135**, 188 (2016).
[64] B. Addison-Jones, K. Tan, B. Yates, J. Cutler, G. Bancroft, and J. Tse, J. Electron Spectrosc. Relat. Phenom. **48**, 155 (1989).
[65] D. Li, G. Bancroft, M. Kasrai, M. Fleet, R. Secco, X. Feng, K. Tan, and B. Yang, Am. Mineral. **79**, 622 (1994).